Electronic Supplementary Material (ESI) for Inorganic Chemistry Frontiers.

Supporting Information

for

Ir_3Pb alloy nanodendrites with high performance for ethanol electrooxidation and their enhanced durability by alloying trace Au

Genlei Zhang, *[, a, b] Zhenxi Zhang [a]

[a] Anhui Province Key Laboratory of Advanced Catalytic Materials and Reaction Engineering, Anhui Province Key Laboratory of Controllable Chemistry Reaction and Material Chemical Engineering, School of Chemistry and Chemical Engineering, Hefei University of Technology, Hefei, 230009, PR China.

[b] School of Materials Science and Engineering, Hefei University of Technology, Tunxi Road 193, Hefei, 230009, PR China.

Corresponding Author

*E-mail: genleizhang@hfut.edu.cn

Number of pages: 32

Number of figures: 19

Number of tables: 6

Note: The figures, tables and text in this Supporting Information document are presented in the order in which they are referenced in the main paper.

Experimental section

Materials

Iridium (III) acetylacetonate (Ir(acac)$_3$), iridium chloride hydrate (IrCl$_3$), lead (II) acetylacetonate (Pb(acac)$_2$), chloroauric acid (HAuCl$_4$), citric acid (CA), poly (vinyl pyrrolidone) (PVP), ascorbic acid (AA), 1-aminopyrene (AP), octadecylamine (ODA), oleylamine (OAm), Ethylene glycol (EG), ethanol, perchloric acid (HClO$_4$) and other chemical reagents were purchased from Sinopharm Chemical Reagent Co. Ltd., China. Poly(vinylpyrrolidone) (PVP, MW≈55000) was purchased from Sigma-Aldrich. Carbon black (Vulcan XC-72), carbon black, commercial carbon supported Pt/C catalyst from Johnson Matthey (Pt/C-JM) and Nafion solution (5 wt%) were purchased from Hesen electric Co. Ltd., China. All aqueous solutions were prepared using deionized (DI) water. High purity nitrogen, argon (N_2, Ar; ≥ 99.99%) and CO (≥ 99.99%) were supplied by Nanjing Special Gas Factory Co., Ltd., China. Glassy carbon electrode (0.071cm^2 in area) was purchased from Tianjin Aida Tech. Co. Ltd., China.

Preparation of Ir$_3$Pb nanoparticles

Typically, 10 mg of IrCl$_3$, 12.5 mg Pb(acac)$_2$, 96 mg of CA and 12 mL of benzyl alcohol were added into a vial (volume: 45 mL). The mixture was transferred into a 48 mL high pressure reaction container, and then heated from room temperature to 180 °C and maintained at 160 °C for 5 h with stirring in an oil bath before it was cooled to room temperature. The resulting Ir$_3$Pb nanoparticles was collected by centrifugation and washed by an ethanol/acetone mixture, and finally dried naturally.

Preparation of Ir/C catalyst

15 mg of IrCl$_3$, 96 mg of CA, 10 mg of carbon black, and 12 mL of benzyl alcohol were

added into a vial. After the vial had been capped, the mixture was ultrasonicated for 1 h. The resulting homogeneous mixture was transferred into a 48 mL high pressure reaction container, and then heated from room temperature to 160 °C and maintained at 160 °C for 5 h with stirring in an oil bath before it was cooled to room temperature. The resulting Ir/C catalyst was collected by centrifugation and washed by an ethanol/acetone mixture, and finally dried naturally. The actual Ir weight content was determined by ICP-AES and the results were displayed in **Table S3**.

Preparation of carbon-supported catalysts

Typically, the obtained porous Ir_3Pb NDs (10 mg in 5 mL cyclohexane) were mixed with carbon black (XC-72, 40 mg) suspended in cyclohexane (10 mL). The mixture was ultrasonicated for 1 h and kept stirring at room temperature overnight. Finally, the ND- Ir_3Pb/C catalyst was separated by centrifugation, washed five times with ethanol/cyclohexane mixture, and re-dispersed in ethanol for electro-catalytic tests. As for porous Ir_3PbAu_x (x = 0.01, 0.05 and 0.1) NDs and Ir_3Pb NPs, the experimental procedure was the same as above, and the ND- Ir_3PbAu_x/C and NP-Ir_3Pb/C catalysts were obtained, respectively. The Ir weight contents for all catalysts were determined by ICP-AES and the results were displayed in **Table S3**.

Characterizations

Transmission electron microscopy (TEM) and high-resolution TEM (HRTEM) were performed using JEOL 2100F microscope (JEOL; Japan) operated at 200 kV. Energy dispersive X-ray spectroscopy (EDS) analysis and high-angle annular dark-field scanning TEM (HAADF-STEM) were also conducted using the same instrument to identify the elemental composition of the products. All the samples for TEM study were prepared by dropping an ethanol diluted suspension of the catalyst onto a copper grid coated with carbon film. The X-ray diffraction (XRD) spectra were conducted via a Rigaku D/Max-2500 X-ray diffractometer (Rigaku; Japan) with a Cu K_{α} source recorded. The X-ray photoelectron spectroscopy (XPS) data were collected using PHI-5000 versa probe (Ulvac-Phi; Japan) with an Al K_{α} source. All the spectra were corrected using C 1s signal located at 284.5 eV. Deconvolution of the spectra was carried out using the software XPS Peak 4.1 with thoroughly considering the constraints on binding energy, peak area and full width at half maximum. Metal contents in all catalysts were determined by the inductively coupled plasma atomic emission spectroscopy (ICP-AES, TJA RADIAL IRIS 1000 ICP-AES).

Electrochemical measurements

The electrochemical measurements were conducted via a PARSTAT 2273 electrochemical workstation at room temperature. A three-electrode system which was composed of a glassy carbon electrode as the working electrode (0.071cm^2 geometric area), a Pt sheet (2×2 cm^2) as counter electrode and a saturated KCl $Hg/HgCl_2$ as reference electrode was employed for the electrochemical test. Typically, the as-prepared catalyst (2.0 mg) and Nafion solution (30 μL, 5.0 wt %) were dissolved in an ethanol aqueous (1 mL, $V_{ethanol}/V_{water} = 1/4$) and then sonicated for 30 min to form a catalyst ink. Next, 3.0 μL of the catalyst ink was dropped onto the polished working electrode and dried in an oven at 60 ºC for about 20 min. The metal mass was obtained from the total amount of catalyst on the electrode and the composition of the catalyst determined by ICP-AES. Prior to electrochemical measurements, the working electrodes are electrochemical activated by sweeping from -0.2 to 1.2 V *vs*. SCE at a scan rate of 50 mV s^{-1} in an N_2-saturated 0.1 M $HClO_4$ solution for 100 cycles. The electrochemically active surface area (EASA) of a catalyst can calculated by measuring the charge collected in the hydrogen adsorption/desorption region after double-layer correction and assuming a value of 210 uC cm^{-2} for the adsorption of a hydrogen monolayer under acid medium. The ethanol electrooxidation was carried out in a N_2-saturated aqueous solution containing 0.1 M $HClO_4$ and 0.1 M ethanol also between -0.2 V and 1.2 V (*vs*. SCE) at a scan rate of 20 mV·s^{-1}. Chronoamperometry (CA) tests were carried out at 0.5 V (*vs*. SCE) for a period of 3600 s. The accelerated durability test was performed by 2000 and 6000 potential cycles between -0.2 and 1.2 V (*vs*. SCE) at 20 mV s^{-1} in N_2-saturated 0.1 M $HClO_4$ solution containing 0.1 M C_2H_5OH. For CO-stripping tests, CO was used to saturate the surface of catalysts by bubbling CO gas in 0.1 M $HClO_4$ while holding the working electrode at -0.14 V *vs*. SCE for 15 min, and then the remaining CO was thoroughly purged with N_2 gas for 15 min. Afterwards, the CO stripping was performed by sweeping from -0.2 to 1.2 V *vs*. SCE at a scan rate of 50 mV s^{-1}.

Electrochemical *in situ* Fourier Transform Infrared Spectroscopy

Electrochemical *in situ* FTIR spectroscopy (*in situ* FTIRs) measurements were conducted on a Nexus 8700 spectrometer (Nicolet) equipped with a liquid nitrogen-cooled MCT-A detector. A CaF2 disk was used as the IR window, and an IR cell with a thin layer configuration between the electrode and the IR window was approached by pushing the electrode against the window before FTIR measurement. *In situ* FTIR spectra were collected using both single potential alteration FTIR spectroscopy (SPAFTIRS). The glassy carbon electrode, platinum black electrode and saturated calomel electrode used as the working electrode, counter electrode and reference electrode during SPAFTIRS experiments, respectively. The resulting spectra were reported as the relative change in reflectivity and calculated as follows:

$$\Delta R/R = (R(E_S)-R(E_R))/R(E_R) \qquad (1)$$

where $R(E_S)$ and $R(E_R)$ are the single-beam spectrum obtained by Fourier transform processing of co-added and averaged interferograms collected at sample potential E_S

and reference potential E_R, respectively.

Supporting Figures

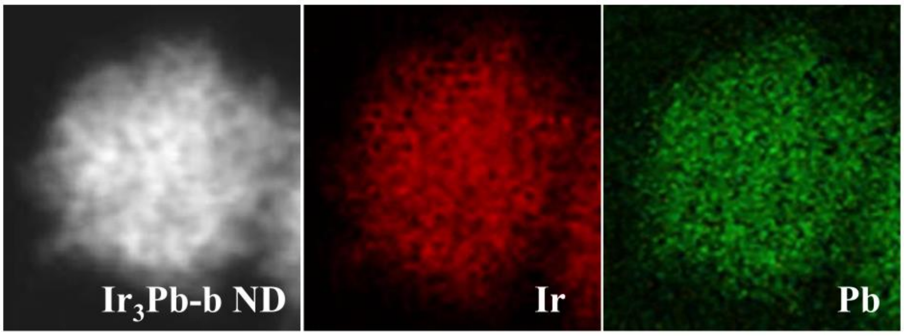

Figure S1 HAADF-STEM image and EDS mapping images of the Ir_3Pb-b NDs.

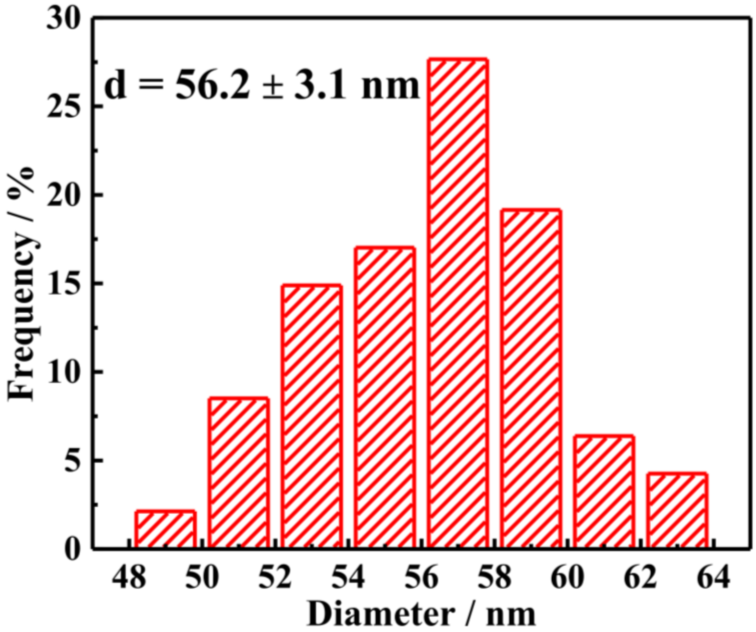

Figure S2 Particle size bar graph of the porous Ir_3Pb NDs.

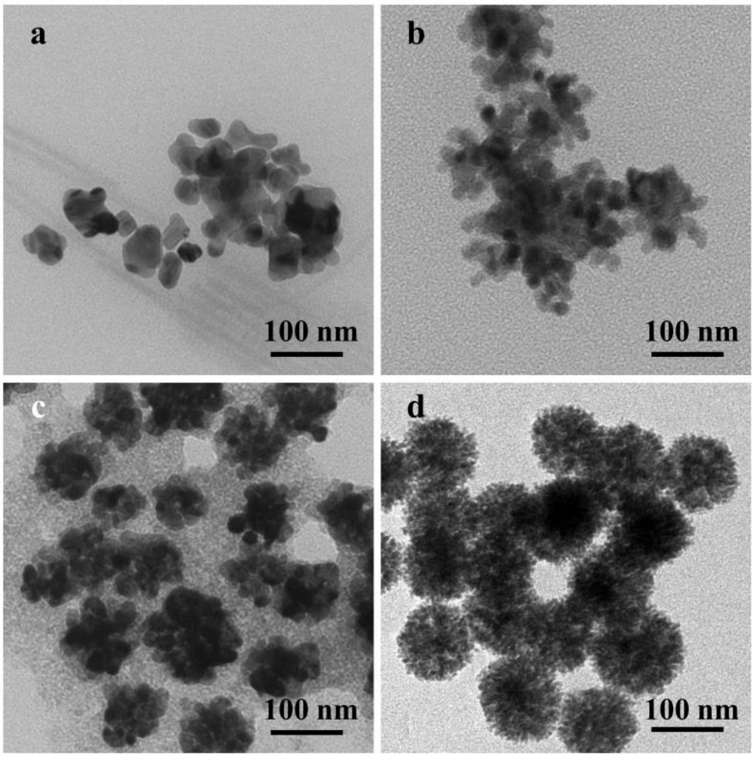

Figure S3 TEM images of the products collected from the reaction with the same condition used in the synthesis of Ir_3Pb NDs but (a) in the absence, (b) 0.2 mg, (c) 0.5 mg and (d) 2.0 mg of AP.

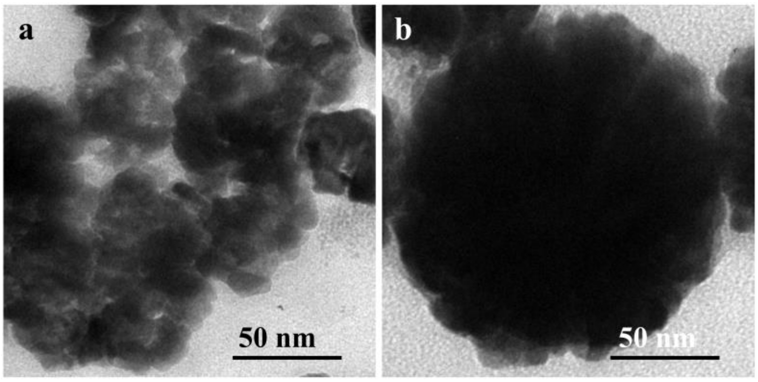

Figure S4 TEM images of the products collected from the reaction with the same condition used in the synthesis of Ir_3Pb NDs but (a) in the absence of PVP and (b) changing PVP into CTAC.

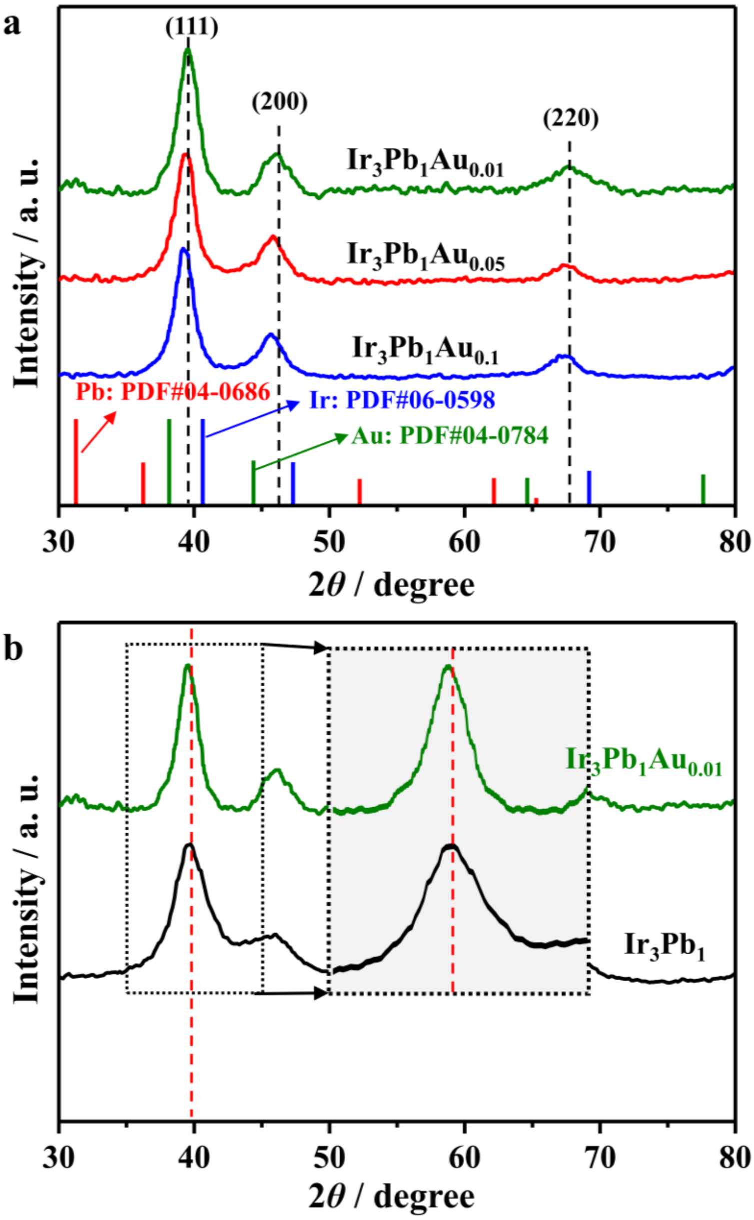

Figure S5 The XRD patterns of the obtained porous $Ir_3PbAu_{0.01}$, $Ir_3PbAu_{0.05}$, $Ir_3PbAu_{0.1}$ and Ir_3Pb NDs.

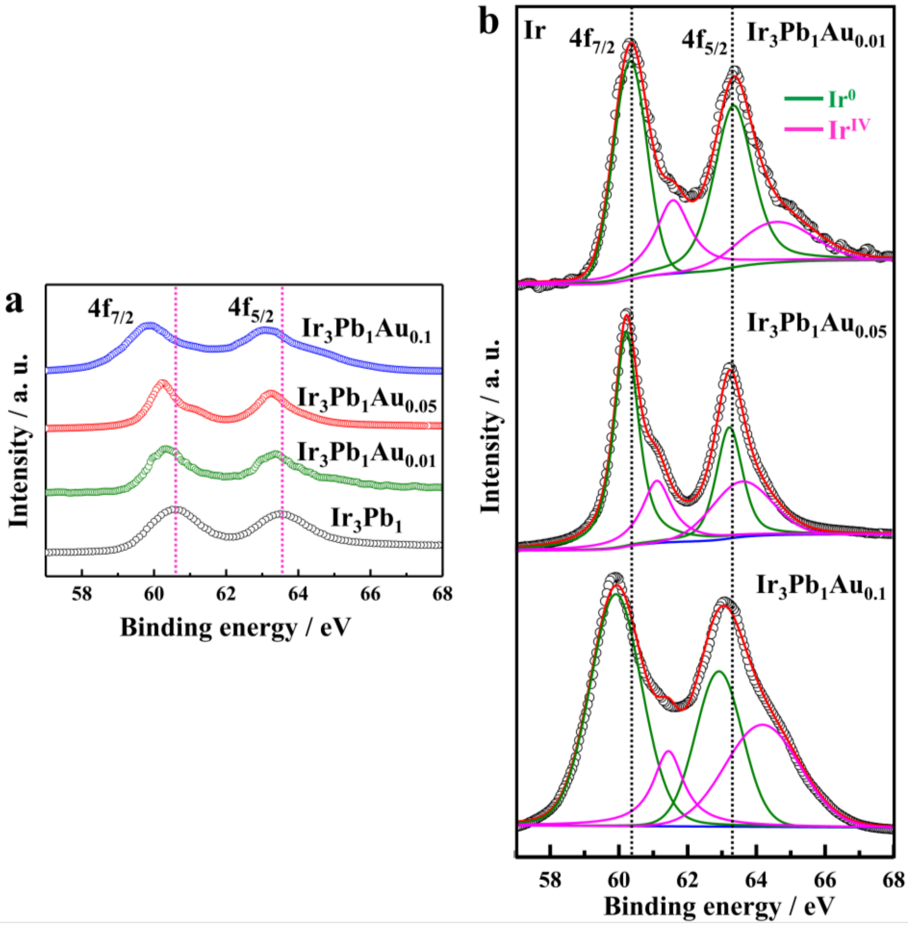

Figure S6 Ir 4f XPS spectra of porous Ir$_3$Pb, Ir$_3$PbAu$_{0.01}$, Ir$_3$PbAu$_{0.05}$, and Ir$_3$PbAu$_{0.1}$ NDs.

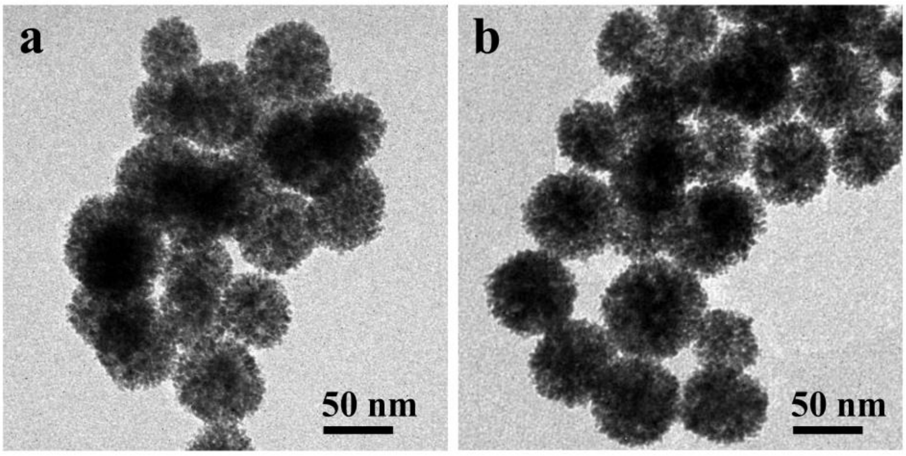

Figure S7 TEM images of $Ir_3PbAu_{0.01}$and $Ir_3PbAu_{0.1}$ NDs.

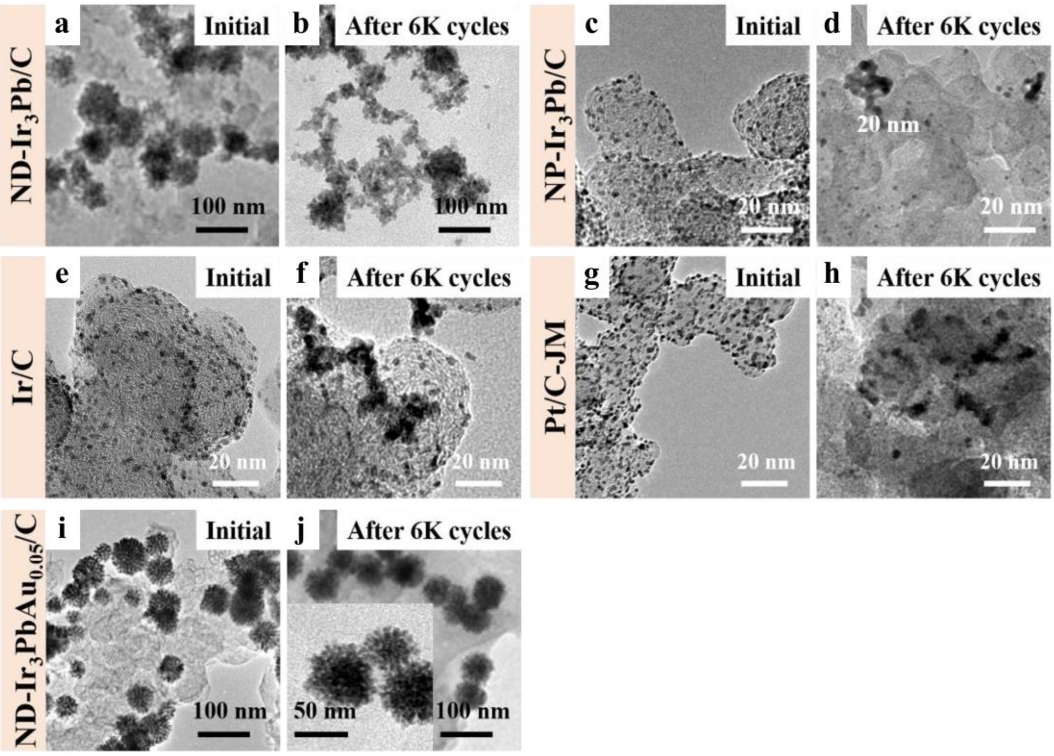

Figure S8 (a, c, e, g, i) TEM images of ND-P-Ir_3Pb/C, NP-Ir_3Pb/C, Ir/C, Pt/C-JM and ND-$Ir_3PbAu_{0.05}$/C; (b, d, f, h, j) TEM images of ND-P-Ir_3Pb/C, NP-Ir_3Pb/C, Ir/C, Pt/C-JM and ND-$Ir_3PbAu_{0.05}$/C after 6000 potential cycles between -0.2 and 1.2 V (*vs.* SCE) at 20 mV s^{-1} in N_2-saturated 0.1 M $HClO_4$ solution containing 0.1 M C_2H_5OH.

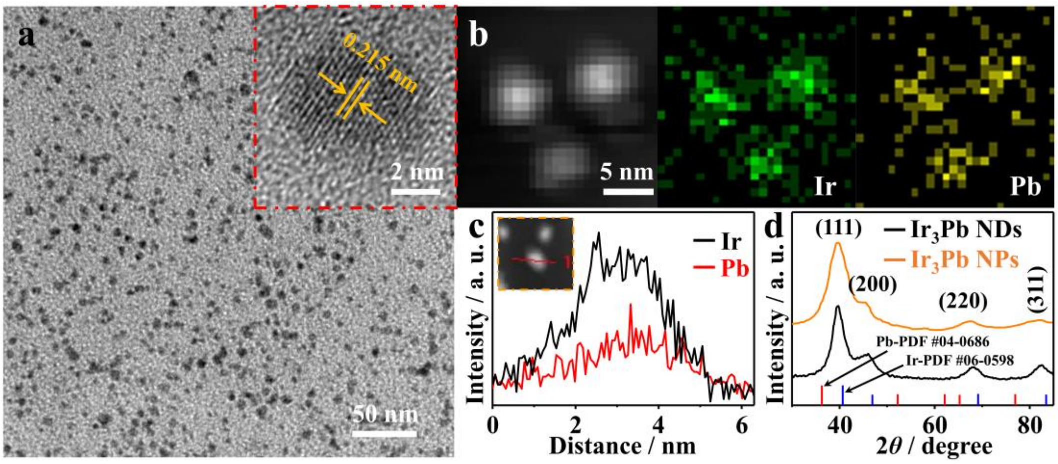

Figure S9 (a) TEM and HRTEM images of the Ir$_3$Pb nanoparticles; (b) HAADF-STEM image and EDS mapping images of the Ir$_3$Pb nanoparticles; (c) HAADF-STEM image and EDS line profiles of a single Ir$_3$Pb nanoparticle; (d) XRD pattern of Ir$_3$Pb nanoparticles.

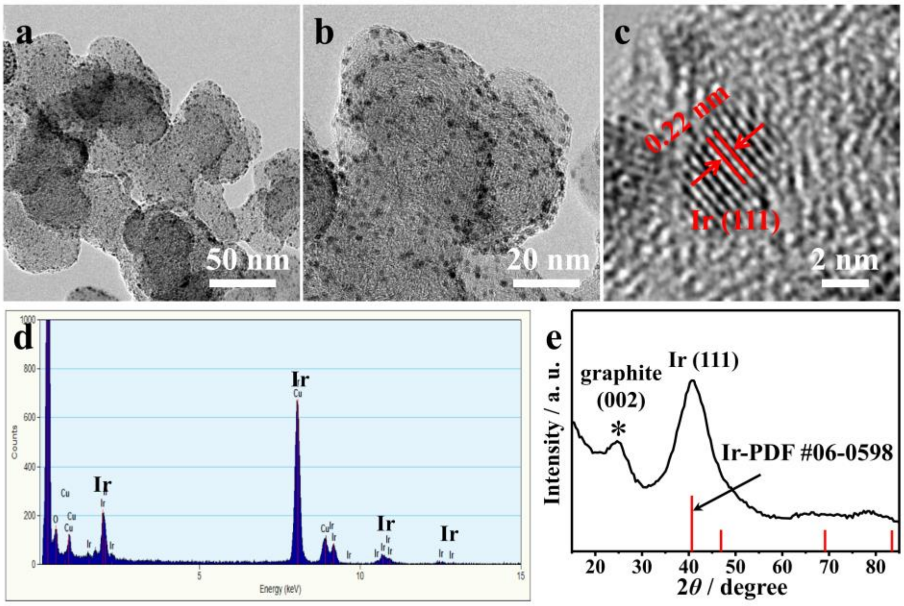

Figure S10 (a-c) TEM and HRTEM images of the Ir/C; (d) EDS and (e) XRD pattern of Ir/C.

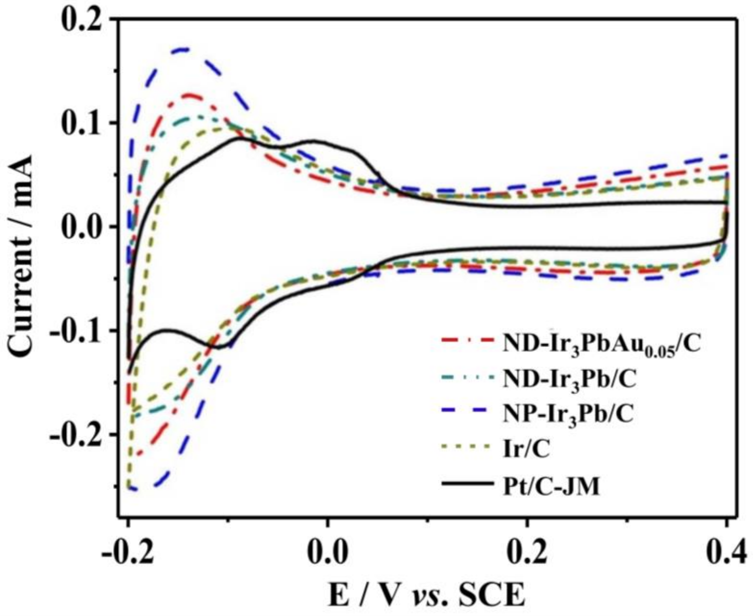

Figure S11 Cyclic voltammograms (between -0.2 to 0.4 V) of ND-Ir$_3$PbAu$_{0.05}$/C, ND-Ir$_3$Pb/C, NP-Ir$_3$Pb/C, Ir/C and Pt/C-JM catalysts in 0.5 M H_2SO_4 electrolyte at scan rate of 20 mV s^{-1}.

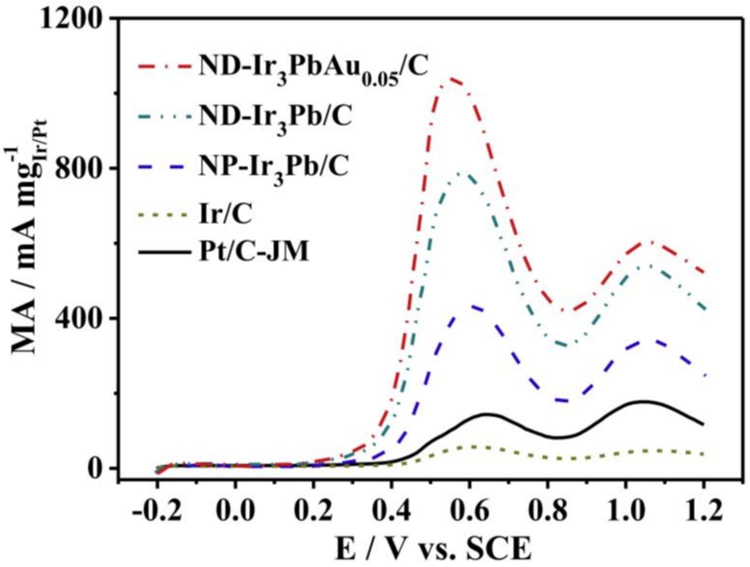

Figure S12 MAs of EOR for ND-$Ir_3PbAu_{0.05}$/C, ND-Ir_3Pb/C, NP-Ir_3Pb/C, Ir/C and Pt/C-JM recorded N_2-saturated 0.1 M $HClO_4$ solution containing 0.1 M C_2H_5OH with a scan rate of 20 mV s^{-1}.

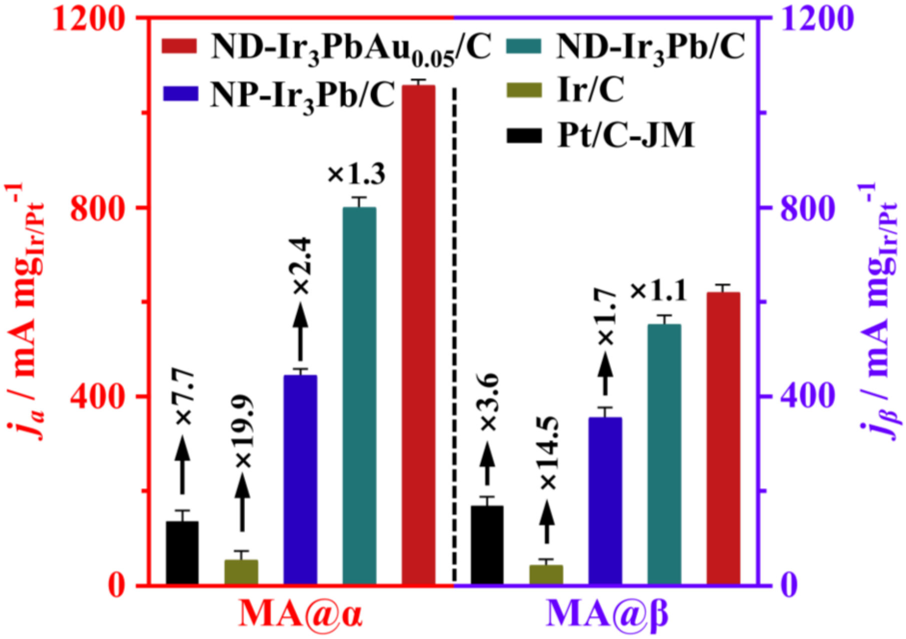

Figure S13 Bar graphs of MAs of ND-$Ir_3PbAu_{0.05}$/C, ND-Ir_3Pb/C, NP-Ir_3Pb/C, Ir/C and Pt/C-JM for j_α and j_β measured in N_2-saturated 0.1 M $HClO_4$ solution containing 0.1 M C_2H_5OH with a scan rate of 20 mV s^{-1}.

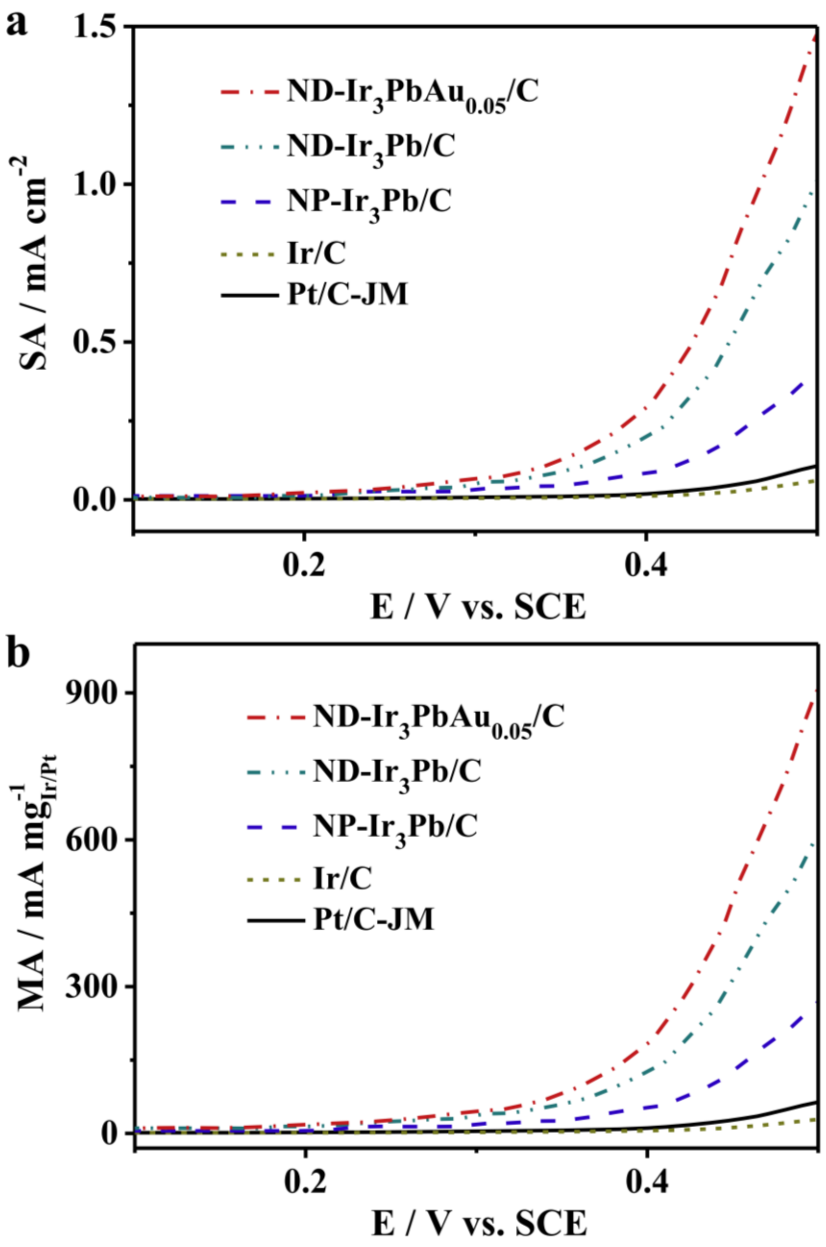

Figure S14 Forward voltammetric scans of ND-Ir$_3$PbAu$_{0.05}$/C, ND-Ir$_3$Pb/C, NP-Ir$_3$Pb/C, Ir/C and Pt/C-JM measured in N$_2$-saturated 0.1 M HClO$_4$ solution containing 0.1 M C$_2$H$_5$OH with a scan rate of 20 mV s^{-1}.

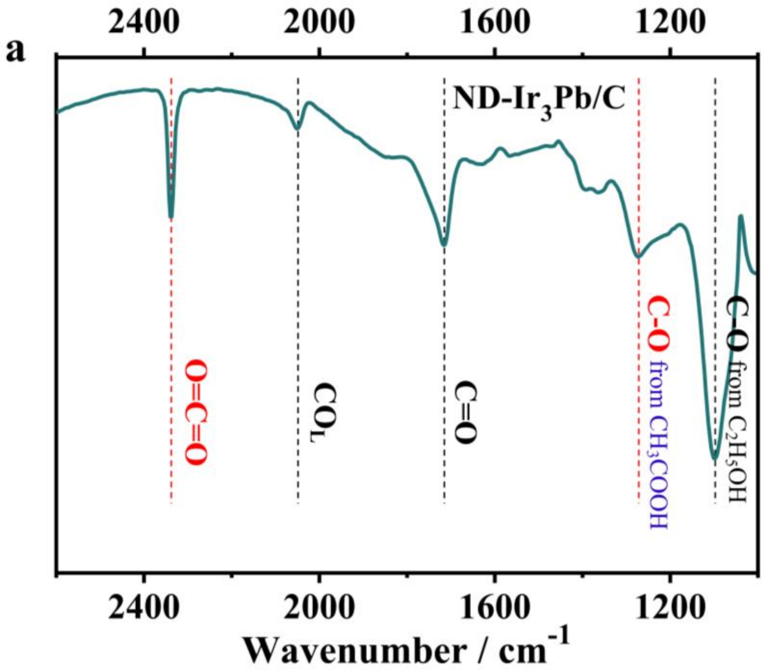

b

Wavenumber / cm^{-1}	Assignment
~ 2345	CO_2 asymmetric stretching
~ 2050	Linearly adsorbed CO_L
~ 1720	C=O stretching of acetaldehyde and acetic acid
~ 1280	C-O stretching of acetic acid
~ 1100	C-O stretching of ethanol

Figure S15 (a) *In situ* FTIR spectra of EOR for the ND-Ir_3Pb/C in 0.1 M $HClO_4$ solution containing 0.1 M C_2H_5OH, E_R = 0.25 V and E_S = 0.6 V. (b) *In situ* FTIR spectra bands assignments.

As shown in **Figure S15**, the band at around 2345 cm^{-1} is a signature peak for the O=C=O asymmetric stretch vibration of CO_2 that comes from completely oxidation of C_2H_5OH, which reflects the cleavage of the C-C bond in ethanol oxidation. The band at around 2050 cm^{-1} can be ascribed to lined bonded CO (CO_L). The band at around 1720 cm^{-1} is the stretching vibration of the C=O bond in CH_3COOH and CH_3CHO because of possible overlap at this wavenumber, which comes from incompletely oxidation of ethanol. A well-defined band at around 1280 cm^{-1} is the characteristic absorption of C-O stretching in CH_3COOH, which is usually used for quantitative evaluation of CH_3COOH. The band at around 1047 cm^{-1} is attributed to the C-O stretching vibration of C_2H_5OH.

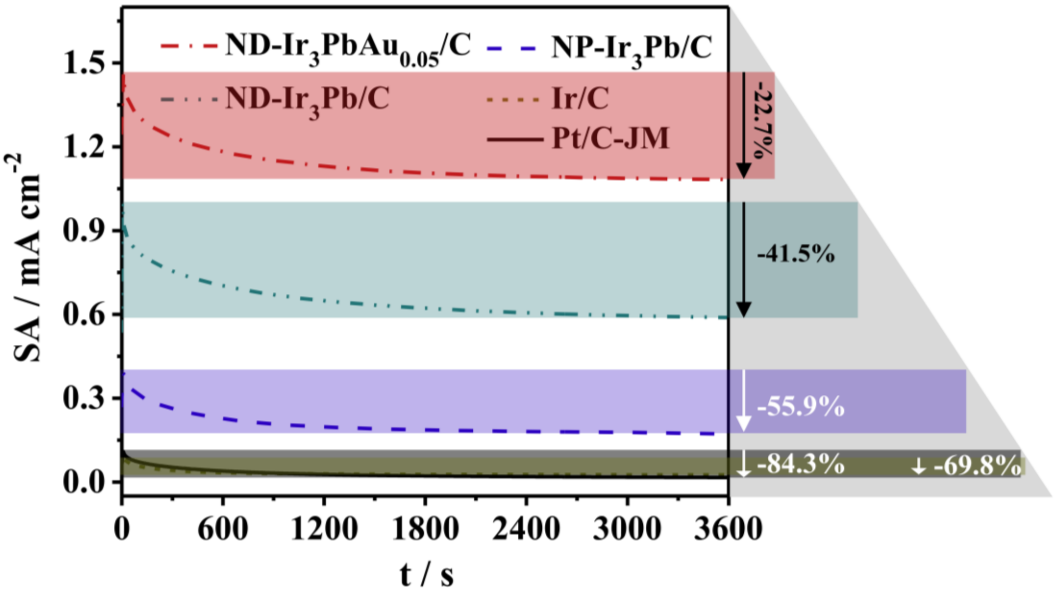

Figure S16 CA curves of ND-$Ir_3PbAu_{0.05}$/C, ND-Ir_3Pb/C, NP-Ir_3Pb/C, Ir/C and Pt/C-JM recorded at 0.5 V (*vs*. SCE).

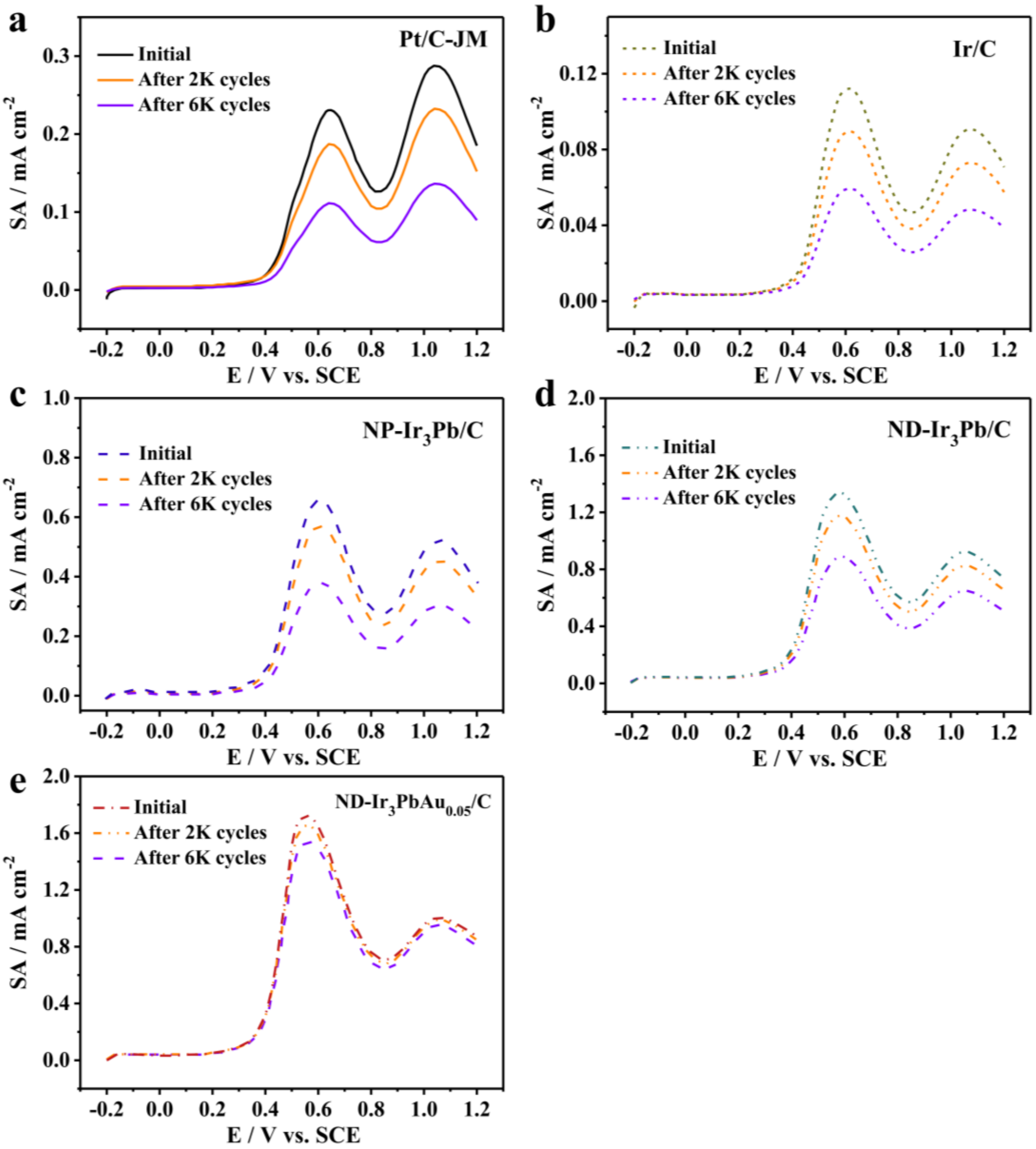

Figure S17 EOR CVs of ND-$Ir_3PbAu_{0.05}$/C, ND-Ir_3Pb/C, NP-Ir_3Pb/C, Ir/C and Pt/C-JM before and after 2000 and 6000 CV cycles in N_2-saturated 0.1 M $HClO_4$ solution containing 0.1 M C_2H_5OH with a scan rate of 20 mV s^{-1}.

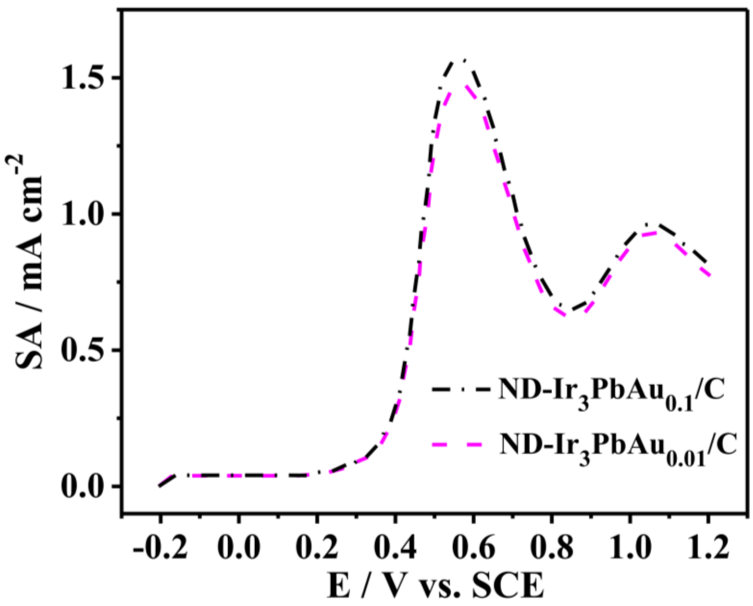

Figure S18 Typical CVs of the ND-Ir$_3$PbAu$_{0.1}$/C and ND-Ir$_3$PbAu$_{0.01}$/C catalysts in N$_2$-saturated 0.1 M HClO$_4$ solution containing 0.1 M C$_2$H$_5$OH with a scan rate of 20 mV s^{-1}.

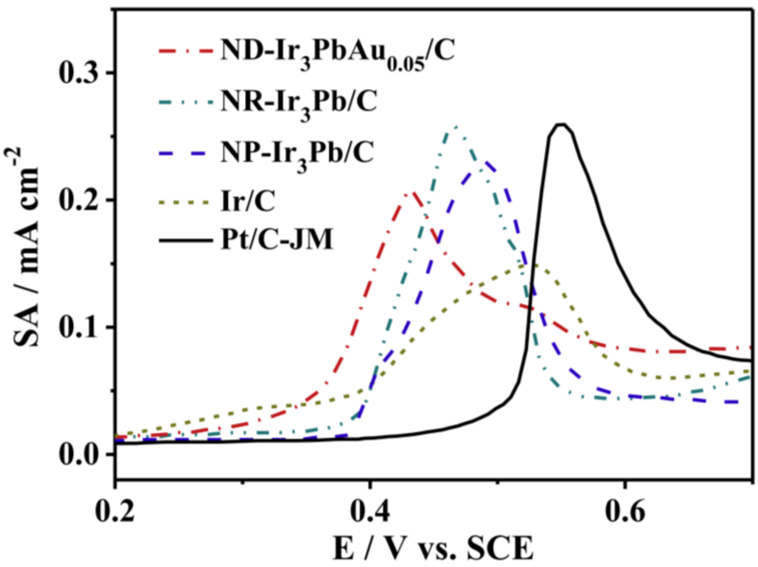

Figure S19 CO stripping voltammograms of ND-$Ir_3PbAu_{0.05}$/C, ND-Ir_3Pb/C, NP-Ir_3Pb/C, Ir/C and Pt/C-JM in 0.1 M $HClO_4$ solution with a scan rate of 50 mV s^{-1}.

Supporting Tables

Table S1 Composition data of samples prepared with different input molar ratio of Ir : Pb on the basis of EDS and ICP-AES analysis.

Input Ir : Pb / mol : mol	**EDS / Ir : Pb (at : at)**		**ICP-AES Ir : Pb (at : at)**
	Experimental ratio	Average ratio	
3 : 0	100 : 0	100 : 0	100 : 0
3 : 1	75.5 : 24.5	(77.2±1.77)	74.3 : 25.7
	79.1 : 20.9	:	
	76.9 : 23.1	(22.8±1.77)	
3 : 2	78.3 : 21.7	(76.9±2.09)	74.8 : 25.2
	74.5 : 25.5	:	
	77.9 : 22.1	(23.1±2.09)	
3 : 3	77.8 : 22.2	(75.7±1.84)	75.1 : 24.9
	74.9 : 25.1	:	
	74.4 : 25.6	(24.3±1.84)	

Table S2 Composition data of the obtained Ir_3Pb NDs, $Ir_3PbAu_{0.1}$ NDs, $Ir_3PbAu_{0.05}$ NDs and $Ir_3PbAu_{0.01}$ NDs on the basis of ICP-AES analysis.

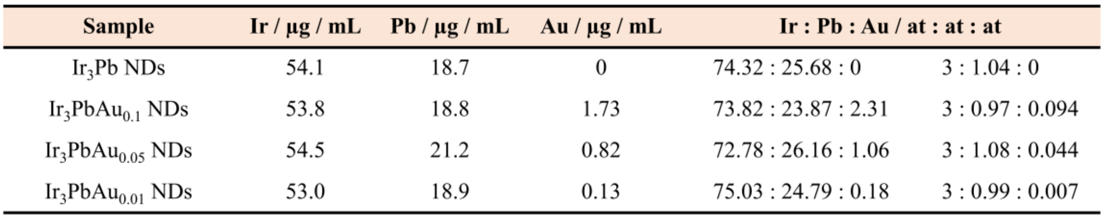

Sample	Ir / µg / mL	Pb / µg / mL	Au / µg / mL	Ir : Pb : Au / at : at : at	
Ir_3Pb NDs	54.1	18.7	0	74.32 : 25.68 : 0	3 : 1.04 : 0
$Ir_3PbAu_{0.1}$ NDs	53.8	18.8	1.73	73.82 : 23.87 : 2.31	3 : 0.97 : 0.094
$Ir_3PbAu_{0.05}$ NDs	54.5	21.2	0.82	72.78 : 26.16 : 1.06	3 : 1.08 : 0.044
$Ir_3PbAu_{0.01}$ NDs	53.0	18.9	0.13	75.03 : 24.79 : 0.18	3 : 0.99 : 0.007

Table S3 The Ir (Pt) loadings of various catalysts on the basis of ICP-AES analysis in this work.

Sample	**Ir (Pt) / wt%**
Pt/C-JM	19.3
Ir/C	18.7
NP-Ir_3Pb/C	18.5
ND-Ir_3Pb/C	17.8
ND-$Ir_3PbAu_{0.1}$/C	19.1
ND-$Ir_3PbAu_{0.05}$/C	18.6
ND-$Ir_3PbAu_{0.01}$/C	18.1

Table S4 The EASA, MA and SA of j_{α} and j_{β}, and the values of j_{α}/j_{β} and $I_{CO2}/I_{CH3COOH}$ of various catalysts in this work.

Sample	**ECSA**	j_{α}		j_{β}		j_{α} / j_{β}	I_{CO_2}/I_{CH_3COOH}
	/ m^2 g$_{Ir\ (Pt)}^{-1}$	**SA / mA cm^{-2}**	**MA / mA mg$_{Ir\ (Pt)}^{-1}$**	**SA / mA cm^{-2}**	**MA / mA mg$_{Ir\ (Pt)}^{-1}$**		
Pt/C-JM	59.62	0.231	137.7	0.288	171.4	0.803	0.75
Ir/C	47.36	0.112	53.2	0.0906	42.9	1.240	1.07
NP-Ir_3Pb/C	66.06	0.674	445.2	0.539	356.1	1.251	1.39
ND-Ir_3Pb/C	59.92	1.337	801.1	0.924	553.6	1.447	2.01
ND-$Ir_3PbAu_{0.05}$/C	61.22	1.732	1060.3	1.015	621.4	1.706	3.09

Table S5 The initial and after 3600s current density of ND-$Ir_3PbAu_{0.05}$/C, ND-Ir_3Pb/C, NP-Ir_3Pb/C, Ir/C and Pt/C-JM in CA.

Catalyst	Current Density / mA cm^{-2}		Loss
	Initial	After 3600 s	
ND-$Ir_3PbAu_{0.05}$/C	1.461	1.129	22.7%
ND-Ir_3Pb/C	1.048	0.613	41.5%
NP-Ir_3Pb/C	0.414	0.183	55.9%
Ir/C	0.062	0.0187	69.8%
Pt/C-JM	0.108	0.0169	84.3%

Table S6 List of up-to-date EOR nanocatalysts reported.

Ref.	**Catalyst**	**Test condition**	**SA / mA cm^{-2}**	**MA / mA mg$_{Ir\ (Pt)}^{-1}$**	**Stability**
Our work	**Ir_3Pb NDs**	**0.1 M $HClO_4$ + 0.1 M C_2H_5OH, 20 mV s^{-1}**	**1.337**	**801.1**	**-34.3 %, 6k cycles**
	$Ir_3PbAu_{0.005}$ NDs		**1.732**	**1060.3**	**-13.9 %, 6k cycles**
1	Carbon supported PtNiCu	0.5 M H_2SO_4 + 1 M C_2H_5OH, 50 mV·s^{-1}	—	634	—
2	PtSn nanosheets	0.5 M H_2SO_4 + 0.5 M C_2H_5OH, 50 mV·s^{-1}	—	292.6	—
3	PtRu nanowires	0.1 M $HClO_4$ + 0.5 M C_2H_5OH, 50 mV s^{-1}	2.08	1550	-49 %, 2k cycles
4	Rh@$Pt_{3.5L}$ nanowires	0.1 M $HClO_4$ + 0.2 M C_2H_5OH, 50 mV s^{-1}	1.18	809	—
5	$Pt_{38}Ir$ nanocubes	0.1 M $HClO_4$ + 0.2 M C_2H_5OH, 50 mV s^{-1}	1.80	—	—
6	Pt-Mo-Ni nanowires	0.5 M H_2SO_4 + 2 M C_2H_5OH, 50 mV s^{-1}	2.57	865.8	—
7	PtRhSn	0.5 M H_2SO_4 + 0.5 M C_2H_5OH, 50 mV s^{-1}	1.78	—	—
8	Pt3RhSn	0.1 M $HClO_4$ + 0.5 M C_2H_5OH, 50 mV s^{-1}	0.19	—	—
9	Pt_3Co@Pt/PC	0.1 M $HClO_4$ + 0.1 M C_2H_5OH, 50 mV s^{-1}	—	790	—
10	Pt_3Sn/C	0.1 M $HClO_4$ + 2 M C_2H_5OH, 50 mV s^{-1}	0.35	—	—
11	Pt nanoflowers	0.1 M $HClO_4$ + 0.1 M C_2H_5OH, 50 mV s^{-1}	1.484	—	—

References

1. Castagna, R. M.; Sieben, J. M.; Alvarez, A. E.; Sanchez, M. D.; Duarte, M. M. E., Carbon supported PtNiCu nanostructured particles for the electro-oxidation of ethanol in acid environment. *Mater. Today Energ.* **2020,** *15*, DOI: 10.1016/j.metener. 2019. 100366.

2. Chen, J. Y.; Lim, S. C.; Kuo, C. H.; Tuan, H. Y., Sub-1nm PtSn ultrathin sheet as an extraordinary electrocatalyst for methanol and ethanol oxidation reactions. *J. Colloid. Interface Sci.* **2019,** *545*, 54-62.

3. Zhu, Y.; Bu, L.; Shao, Q.; Huang, X., Subnanometer PtRh nanowire with alleviated poisoning effect and enhanced C-C bond cleavage for ethanol oxidation electrocatalysis. *ACS Catal.* **2019,** *9* (8), 6607-6612.

4. Liu, K.; Wang, W.; Guo, P.; Ye, J.; Wang, Y.; Li, P.; Lyu, Z.; Geng, Y.; Liu, M.; Xie, S., Replicating the defect structures on ultrathin Rh nanowires with Pt to achieve superior electrocatalytic activity toward ethanol oxidation. *Adv Funct. Mater.* **2019,** *29* (2), 1806300.

5. Chang, Q.; Kattel, S.; Li, X.; Liang, Z.; Tackett, B. M.; Denny, S. R.; Zhang, P.; Su, D.; Chen, J. G.; Chen, Z., Enhancing C-C bond scission for efficient ethanol oxidation using PtIr nanocube electrocatalysts. *ACS Catal.* **2019,** *9* (9), 7618-7625.

6. Mao, J. J.; Chen, W. X.; He D. S.; Wan, J. W.; Pei, J. J.; Dong, J. C.; Wang, Y.; An, P. F.; Jin, Z.; Xing, W.; Tang, H. L.; Zhuang, Z. B.; Liang, X.; Huang, Y.; Zhou, G.; Wang, L. Y.; Wang, D. S.; Li, Y. D., Design of ultrathin Pt-Mo-Ni nanowire catalysts for ethanol electrooxidation. *Sci. Adv.* **2017**, *3* (8), 1603068.

7. Erini, N.; Loukrakpam, R.; Petkov, V.; Baranova, E. A.; Yang, R.; Teschner, D.; Huang, Y.; Brankovic, S. R.; Strasser, P., Ethanol Electro-Oxidation on Ternary Platinum–Rhodium–Tin Nanocatalysts: Insights in the Atomic 3D Structure of the Active Catalytic Phase. *ACS Catal.* **2014,** *4* (6), 1859-1867.

8. Dai, L. X.; Wang, X. Y.; Yang, S. S.; Zhang, T.; Ren, P. J.; Ye, J. Y.; Nan, B.; Wen, X. D.; Zhou, Z. Y.; Si, R.; Yan, C. H.; Zhang, Y. W., Intrinsic composition and electronic effects of multicomponent platinum nanocatalysts with high activity and selectivity for

ethanol oxidation reaction. *J. Mater. Chem. A* **2018,** *6* (24), 11270-11280.

9. Zhang, B. W.; Sheng, T.; Wang, Y. X.; Qu, X. M.; Zhang, J. M.; Zhang, Z. C.; Liao, H. G.; Zhu, F. C.; Dou, S. X.; Jiang, Y. X.; Sun, S. G., Platinum-cobalt bimetallic nanoparticles with Pt skin for electro-oxidation of ethanol. *ACS Catal.* **2016,** *7* (1), 892-895.

10. Kwak, D. H.; Lee, Y. W.; Han, S. B.; Hwang, E. T.; Park, H. C.; Kim, M. C.; Park, K. W., Ultrasmall PtSn alloy catalyst for ethanol electro-oxidation reaction. *J. Power Sources* **2015,** *275*, 557-562.

11. Wei, L.; Fan, Y. J.; Wang, H. H.; Tian, N.; Zhou, Z. Y.; Sun, S. G., Electrochemically shape-controlled synthesis in deep eutectic solvents of Pt nanoflowers with enhanced activity for ethanol oxidation. *Electrochimica Acta* **2012,** *76*, 468-474.